

Towards room temperature ionic liquid crystals: linear *versus* bent imidazolium phenylpyrimidines†

Gundula F. Starkulla, Simon Klenk, Martin Butschies, Stefan Tussetschläger and Sabine Laschat*

Received 13th July 2012, Accepted 17th August 2012

DOI: 10.1039/c2jm34595a

The synthesis and the mesomorphic properties of novel imidazolium salts with mesogenic 2-phenylpyrimidine or 2-alkylpyrimidincarboxylic acid central cores are reported. The mesogenic units are connected to the imidazolium head groups *via* an alkoxy spacer. In order to adjust the mesomorphic properties the length of the alkoxy spacer and the terminal alkyl group, the counter ion, the substitution pattern of the imidazolium head group and the molecular geometry (linear *vs.* bent) are varied and the corresponding compounds were investigated in detail using differential scanning calorimetry (DSC), polarized optical microscopy (POM) and X-ray scattering (WAXS, SAXS). Whereas SmA phases with monolayer orientation were observed for imidazolium salts with short *N*-substituents ($R = \text{CH}_3, \text{C}_4\text{H}_9$) at the imidazolium head group, the corresponding derivatives with longer *N*-substituents ($R = \text{C}_{12}\text{H}_{25}, \text{C}_{12}\text{H}_{25}\text{OC}_6\text{H}_4$) displayed SmA phases with bilayer orientation irrespective of a linear or bent geometry. For two derivatives, *p*-5(10,8) and *p*-5(12,8), a SmC phase was observed. Indeed, bending of the mesogenic core led to a shift of the mesophases towards lower temperatures. Several of the *meta*-2-phenylpyrimidine derivatives as well as 2-pyrimidine carboxylates displayed melting points below 50 °C. For 2-pyrimidine carboxylates replacement of a bromide anion by triflate resulted in a further decrease of the melting transition close to ambient temperature.

Introduction

Ionic liquids (ILs) are molten salts, in which either the cation or the anion or both are organic compounds and which are firmly established for both laboratory as well as industrial applications due to their promising properties such as high chemical and thermal stability, non-volatility, non-flammability, high ionic conductivity and broad electrochemical window.¹ It has been fully recognized only recently that ionic liquid crystals (ILCs), *i.e.* ionic liquids with liquid crystalline properties, not only combine the best of two worlds, *i.e.* ILs and liquid crystals (LCs),² but display additional features which are not observed in ILs or LCs alone, *e.g.*, one dimensional ionic conductivity.³ Thus, ILCs can be considered as charged supramolecular ordered systems whose mesomorphic properties, *i.e.* mesophase type, packing symmetry, and phase transition temperatures, can be adjusted by the type of anions/cations, mesogenic subunits, substitution patterns and additives although a *de novo* design of certain properties is still out of reach.

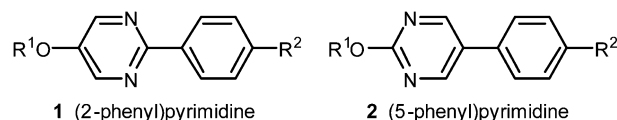
Calamitic thermotropic liquid crystals consist of a large variety of structurally different mesogenic cores, in which both 2- and

5-phenylpyrimidines **1** and **2** (Scheme 1) are prominent members.⁴ The nitrogen atoms introduce lateral polarity which is favourable for the formation of SmC phases while retaining a rod-like structure resulting in low viscosity materials. Thus, phenylpyrimidines are widely applied as ferroelectric host materials.^{4,5}

Furthermore, 2- and 5-phenylpyrimidines, **1** and **2**, are not just regioisomers, but they differ in their conformation.^{6,7} For 2-phenylpyrimidine **1** a planar conformation is favoured while the corresponding 5-phenylpyrimidine **2** is twisted due to steric hindrance between lateral *ortho*-hydrogen atoms. Therefore, it is not surprising that the regioisomers also differ in their mesomorphic properties, as observed by Lemieux and Tschierske.^{8,9}

Despite ample precedence of ionic liquid crystals containing biphenyls as calamitic units,³ the corresponding phenylpyrimidines **3** (Scheme 2) have only been rarely employed for such purposes.¹⁰

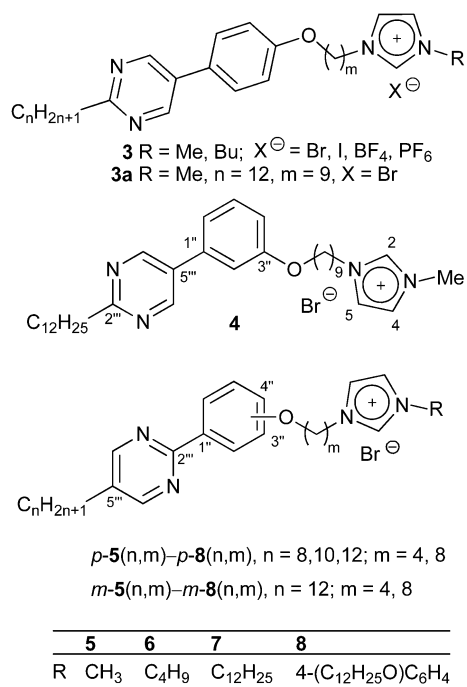
We have recently reported the mesomorphic properties of 5-phenylpyrimidines **3** with a tethered imidazolium moiety with respect to chain lengths, tether lengths and counter ions.¹⁰



Scheme 1

Institut für Organische Chemie, Universität Stuttgart, Pfaffenwaldring 55, 70569 Stuttgart, Germany. E-mail: sabine.laschat@oc.uni-stuttgart.de; Fax: +49-711-685-64285; Tel: +49-711-685-64565

† Electronic supplementary information (ESI) available. See DOI: 10.1039/c2jm34595a



Scheme 2

Although *N*-methylimidazolium bromides **3** ($n = 12$, $m = 4-9$) displayed broad mesophase ranges (SmA), the high clearing temperatures affected the thermal stability considerably and led to decomposition after repetitive heating/cooling cycles. In addition melting points were relatively high, thus limiting the potential applications of these novel materials.

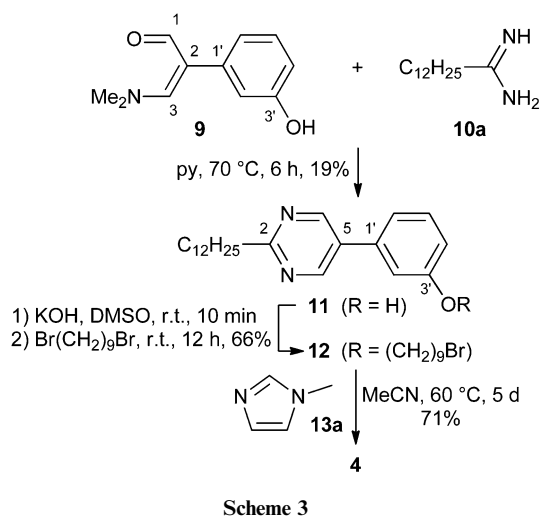
In order to shift the mesophase towards ambient temperature we anticipated that a bent geometry of the calamitic phenylpyrimidine *via a meta-* rather than a *para*-substitution pattern should be a suitable approach for such purposes. From ionic liquids it is well known that reduction of symmetry leads to a decrease of melting points.¹¹ In addition the corresponding linear 2-phenylpyrimidines *p-5(n,m)-p-8(n,m)* and bent 2-phenylpyrimidines *m-5(n,m)-m-8(n,m)* were investigated for comparison. The results are reported below.

Results and discussion

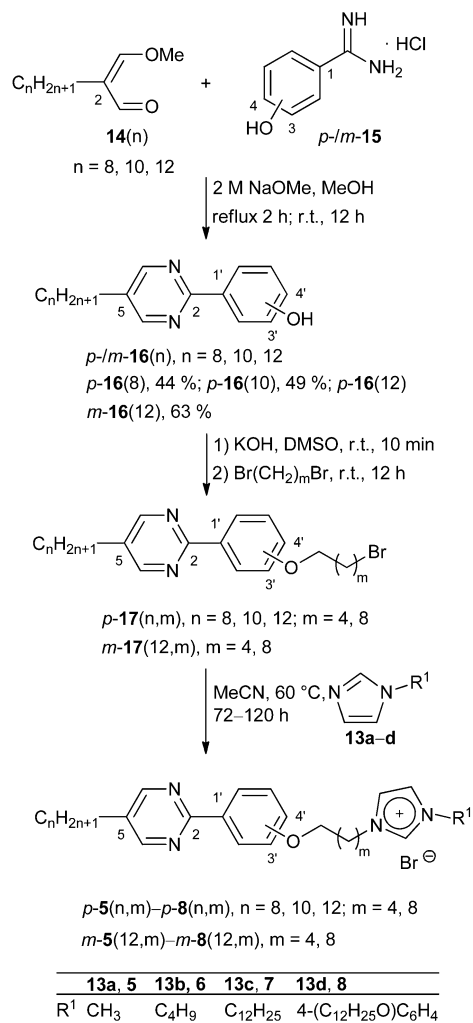
Following our previously established procedure, enamine **9**¹² was submitted to condensation with dodecanamide **10a**¹³ to give 3-(2-dodecylpyrimidin-5-yl)phenol **11**.^{10,14} Subsequent etherification with 1,9-dibromononane gave bromide **12**, which was alkylated with *N*-methylimidazole **13a** to yield the desired bent 5-phenylpyrimidine **4** (Scheme 3).

However, due to the very poor yield of key intermediate **11** we abandoned this route and decided to look into more detail of the corresponding linear and bent 2-phenylpyrimidines *p-5(n,m)-p-8(n,m)* and *m-5(n,m)-m-8(n,m)*, respectively. For the synthesis of 2-phenylpyrimidines *p-5(n,m)-p-8(n,m)* the inverse route was chosen as compared to 5-phenylpyrimidines (Scheme 4).

Enoethers **14(n)**, being accessible from dimethyl acetals according to a literature procedure,¹⁵ were condensed with 4-hydroxybenzenecarboximidamide hydrochloride *p-15*, which is



commercially available^{16a} or can be easily prepared from 4-cyanophenol *via* ammonolysis,^{16b} to afford 4-(5-alkylpyrimidin-2-yl)phenols *p-16(n)*. Further Williamson etherification gave the respective bromides *p-17(n,m)*. The latter was treated with



Scheme 4 Preparation of 2-phenylpyrimidines *p-5(n,m)-p-8(n,m)* and *m-5(12,m)-m-8(12,m)* (numbering for NMR assignment).

N-alkylimidazoles **13a–d** to afford the desired target compounds *p*-**5**(*n,m*)–*p*-**8**(*n,m*). In the case of *meta*-substituted 2-phenylpyrimidines, only derivatives *m*-**5**(12,*m*)–*m*-**8**(12,*m*) with the most promising chain length C12 at the pyrimidine moiety were prepared in an analogous manner by condensation of **14**(12) and *m*-**15**, followed by etherification and reaction with *N*-alkylimidazoles **13a–d** (Scheme 4).

Mesomorphic properties of compounds **4**, *p*-**5**(*n,m*)–*p*-**8**(*n,m*) were investigated by differential scanning calorimetry (DSC), polarizing optical microscopy (POM) and X-ray diffraction (WAXS and SAXS). The DSC results are summarized in Table 1.

Comparison of the known *para*-substituted 5-phenylpyrimidine **3a**¹⁰ with the corresponding *meta*-substituted 5-phenylpyrimidine **4** revealed a decrease of both melting and clearing temperatures from 72 °C and 169 °C to 34 °C and 114 °C, respectively (entries 1 and 2). As mentioned above, the poor yield of **4** precluded the access to other derivatives of this series and thus, we focused on the 2-phenylpyrimidines. *Para*-substituted 2-phenylpyrimidines *p*-**5**(8,4)–*p*-**5**(12,4) with a methylimidazolium unit and a C4 spacer displayed melting points between 89 and 112 °C and clearing points between 190–255 °C (entries 3–5). Increasing the spacer length to C8 had only a little effect on the melting temperatures, but decreased the clearing transitions to 148–197 °C (entries 6–8). However, the most surprising effect was that compounds *p*-**5**(10,8) and *p*-**5**(12,8) displayed a SmC phase (71–98 °C and 104–116 °C) in addition to the SmA phase

(98–177 °C and 116–197 °C) (entries 7 and 8). It should be noted that SmC phases are relatively uncommon for ionic liquid crystals.¹⁷

One possible reason for the observation of SmC phases of compounds *p*-**5**(10,8) and *p*-**5**(12,8) might be that, for these particular spacer and chain length combinations, the “SmC promoting effect” of phenylpyrimidines, reported by Lemieux,^{4,8a} seems to overrule any other mesophase-controlling effects. The finding that compound *p*-**5**(10,8) has a lower melting point as compared to compound *p*-**5**(8,8) (entries 6 and 7) might be explained as follows. In the case of *p*-**5**(10,8) the melting transition from Cr to SmC presumably requires less energy as compared to the melting transition from Cr to SmA in the case of *p*-**5**(8,8).

Extending the lengths of the substituent at the imidazolium unit has considerable influence on the mesomorphic properties. Within the *N*-butylimidazolium series derivatives *p*-**6**(8,4), *p*-**6**(10,4) and *p*-**6**(8,8) are non-mesomorphic, while compounds *p*-**6**(12,4), *p*-**6**(10,8) and *p*-**6**(12,8) display SmA mesophases with much lower melting (46–69 °C) and clearing temperatures (87–113 °C) (entries 9–14) as compared to the corresponding *N*-methylimidazolium salts *p*-**5**(12,4), *p*-**5**(10,8) and *p*-**5**(12,8). A further extension of the lengths of the *N*-substituent gives a different result. While melting points either decreased only slightly for the C4 spacer on the *N*-dodecylimidazolium series *p*-**7**(*n,m*), and increased for the C8 spacer (entries 15–20), clearing

Table 1 Phase transition temperatures (°C) and transition enthalpies (kJ mol⁻¹) of compounds **3**, **4** and *p*-**5**(*n,m*)–*p*-**8**(*n,m*) with different side chains, tether lengths and *N*-substituents

Entry	Compound	R ¹	Cr	SmC	SmA	I	Heating/cooling		
1	3a ^a	CH ₃	•	72 (25.7)	—	•	169 (0.6)	•	2. Heating
2	4	CH ₃	•	34 (16.6)	—	•	114 (0.3)	•	2. Heating
3	<i>p</i> - 5 (8,4)	CH ₃	•	99 (9.6)	—	•	190 (0.8)	•	2. Heating
4	<i>p</i> - 5 (10,4) ^b	CH ₃	•	89 (6.4)	—	•	220 (0.5)	•	1. Heating
5	<i>p</i> - 5 (12,4) ^b	CH ₃	•	112 (21.5)	—	•	255 (0.7)	•	1. Heating
6	<i>p</i> - 5 (8,8)	CH ₃	•	88 (18.7)	—	•	148 (0.9)	•	2. Heating
7	<i>p</i> - 5 (10,8)	CH ₃	•	71 (25.1)	•	•	177 (0.7)	•	2. Heating
8	<i>p</i> - 5 (12,8)	CH ₃	•	104 (48.0)	•	•	197 (0.7)	•	2. Heating
9	<i>p</i> - 6 (8,4)	C ₄ H ₉	•	56 (13.2)	—	—	—	•	1. Heating ^c
10	<i>p</i> - 6 (10,4)	C ₄ H ₉	•	97 (15.1)	—	—	—	•	2. Heating
11	<i>p</i> - 6 (12,4)	C ₄ H ₉	•	46 (2.7)	—	•	113 (0.4)	•	2. Heating
12	<i>p</i> - 6 (8,8)	C ₄ H ₉	•	82 (3.7)	—	—	—	•	2. Heating
13	<i>p</i> - 6 (10,8)	C ₄ H ₉	•	54 (21.7)	—	•	87 (6.1)	•	2. Heating
14	<i>p</i> - 6 (12,8)	C ₄ H ₉	•	69 (4.0)	—	•	106 (1.0)	•	2. Heating
15	<i>p</i> - 7 (8,4)	C ₁₂ H ₂₅	•	110 (23.9)	—	—	—	•	2. Heating
			•	93 (−27.0)	—	•	100 (−1.8)	•	2. Cooling
16	<i>p</i> - 7 (10,4)	C ₁₂ H ₂₅	•	112 (54.9)	—	—	—	•	2. Heating
			•	106 (−30.4)	—	•	116 (−1.8)	•	2. Cooling
17	<i>p</i> - 7 (12,4)	C ₁₂ H ₂₅	•	111 (30.9)	—	•	125 (1.7)	•	2. Heating
18	<i>p</i> - 7 (8,8)	C ₁₂ H ₂₅	•	74 (42.1)	—	•	79 (1.7)	•	2. Heating
19	<i>p</i> - 7 (10,8)	C ₁₂ H ₂₅	•	78 (54.9)	—	—	—	•	2. Heating
			•	65 (−50.7)	—	•	82 (−3.6)	•	2. Cooling
20	<i>p</i> - 7 (12,8)	C ₁₂ H ₂₅	•	81 (53.2)	—	—	—	•	2. Heating
21	<i>p</i> - 8 (8,4)	Ar	•	158 (35.2)	—	•	190 (2.4)	•	2. Heating
22	<i>p</i> - 8 (10,4)	Ar	•	156 (38.7)	—	•	204 (2.3)	•	2. Heating
23	<i>p</i> - 8 (12,4)	Ar	•	143 (34.2)	—	•	195 (1.9)	•	2. Heating
24	<i>p</i> - 8 (8,8)	Ar	•	158 (37.8)	—	—	—	•	2. Heating
25	<i>p</i> - 8 (10,8)	Ar	•	164 (40.7)	—	—	—	•	2. Heating
			•	137 (−38.6)	—	•	142 (−1.3)	•	2. Cooling
26	<i>p</i> - 8 (12,8)	Ar	•	99 (6.9)	—	—	—	•	2. Heating

^a Values from ref. 10. ^b Decomposition after 1. heating. ^c No mesophases were detected. Ar = C₁₂H₂₅OC₆H₄, Cr = crystalline, SmC = smectic C, SmA = smectic A, and I = isotropic. Dot = phase was observed; dash = phase was not observed.

points were shifted significantly to lower temperatures, resulting in the complete loss of mesophases for *p*-7(8,4), *p*-7(10,4), *p*-7(10,8), *p*-7(12,8) and a decrease of the mesophase width for *p*-7(12,4) and *p*-7(8,8). For *p*-7(8,4), *p*-7(10,4) and *p*-7(10,8) SmA mesophases were observed only upon second cooling from the isotropic liquid (entries 15, 16, and 19). This counterbalance of spacer lengths versus the *N*-substituent size can also be observed for the series *p*-8(*n*,*m*) with a more rigidified *N*-(4-dodecyloxyphenyl)imidazolium unit (entries 21–26). Melting points are significantly increased to 99–164 °C as compared to the *N*-methylimidazolium series *p*-5(*n*,*m*) regardless of the spacer. Clearing points, however, remained high for the C4 spacer as observed for the *N*-methyl series *p*-5(*n*,4), while a decrease of clearing temperatures for the C8 spacer resulted in the complete loss of mesomorphism. Only derivative *p*-8(10,8) displayed a SmA mesophase over a small temperature range of 5 K upon second cooling.

The effect of the spacer versus the *N*-substituent for *meta*-substituted 2-phenylpyrimidines *m*-5(12,*m*)–*m*-8(12,*m*) is given in Table 2.

Comparison of the results for these compounds with the corresponding *para*-substituted series *p*-5(12,*m*)–*p*-8(12,*m*) clearly revealed a decrease of both melting and clearing points with the effect being most pronounced for compound *m*-5(12,8) albeit at the loss of the SmC phase, which is present in *p*-5(12,8). In the case of *m*-6(12,4), any mesomorphism totally disappeared and in *m*-7(12,8) the mesophase width was decreased to a range of only 4 K. Typical DSC traces are given in Fig. 1.

Under POM, samples of compounds *p*-5(10,8) and *p*-5(12,8), which were slowly cooled from the isotropic mixture, showed homeotropic alignment and dichroism was only visible at the air–liquid interface of air bubbles. By shearing of the homeotropic textures lamellar textures could be generated. For compounds *p*-5(10,8) and *p*-5(12,8) the phase transition from SmA to SmC was clearly visible under POM. Upon cooling from the isotropic phase, homeotropic textures of the SmA phase were observed, which turned into a non-characteristic texture at 110 °C and became a Schlieren texture at 105 °C typical for a SmC phase (Fig. 2).¹⁸

XRD studies of selected compounds *p*-5(12,4), *p*-5(8,8), *p*-5(10,8), *p*-5(12,8), *p*-6(12,8), *p*-7(12,4), *p*-8(12,4), *m*-5(12,4) and *m*-7(12,4) revealed diffraction patterns typical for smectic mesophases, with a strong fundamental diffraction peak (001), in

some cases small second-order (002) and third-order (003) peaks, and the diffuse scattering from the alkyl chains around 4.8 Å. The first order peaks (001) were fit with a Gaussian distribution to obtain the exact d_{001} values (the whole XRD data can be found in the ESI†). Two typical diffractograms are shown in Fig. 3 and 4.

Compounds *p*-5(8,8)–*p*-5(12,8) were also investigated in temperature-dependent XRD experiments to confirm the above-mentioned observations under POM. While both compounds *p*-5(10,8) and *p*-5(12,8) displayed slightly increasing layer spacings within the SmC phase and strongly decreasing layer spacings in the SmA phases upon raising the temperature, only a SmA phase with much less temperature-dependent layer spacing was observed for compound *p*-5(8,8) (Fig. 5). The negative thermal expansion within the SmA phase results from the loss of orientational order upon raising the temperature.^{19,20} It should be noted that this behavior already has been observed previously.^{21,22}

Further temperature-dependent measurements for compounds *p*-6(12,8), *p*-7(12,4), *p*-8(12,4), *m*-5(12,4) and *m*-7(12,4) have been done (see ESI†). To assign whether the molecules are packed in mono- or bilayers within the smectic mesophases, the experimental data (see ESI†) were interpolated to determine the d_{001} values at a reduced temperature near the clearing point ($T = 0.95 \times T_{\text{iso}}$) and the results were compared to the molecular length calculated with Chem3D²³ (Table 3).

For derivatives *p*-5(10,8) and *p*-5(12,8) displaying an additional SmC mesophase the experimentally determined d_{001} values were also interpolated to temperatures near the SmA/SmC phase transition ($T = 1.05 \times T_{\text{SmC/SmA}}$ and $T = 0.95 \times T_{\text{SmC/SmA}}$). As expected the d_{001} values significantly increase from 5724 pm for *p*-5(10,8) and 5982 pm for *p*-5(12,8) (both at $T = 0.95 \times T_{\text{SmC/SmA}}$) to 6432 pm for *p*-5(10,8) and 6486 pm for *p*-5(12,8) (both at $T = 1.05 \times T_{\text{SmC/SmA}}$) at the transition from the smectic C to the smectic A phase (Table 3).

For all mesophases of compounds *p*-5(12,4), *p*-5(8,8), *p*-5(10,8), *p*-8(12,8), *p*-6(12,8) and *p*-5(12,4) with short tails at the imidazolium head group (*N*-Me, *N*-Bu) the quotient of the observed layer spacing and the calculated molecular length is larger than 1, while it is smaller than 1 for compounds *p*-7(12,4), *p*-8(12,4) and *m*-7(12,4) with larger tails (*N*-*n*-C₁₂H₂₅, *N*-4-C₆H₄OC₁₂H₂₅) attached to the head group. We therefore propose smectic bilayers with interdigitated alkyl chains for the former ones and smectic monolayers for the latter ones. The formation of smectic bilayers where the ionic head groups of the molecules are stacked towards each other seems to be only favored for compounds with small chains ($R^1 = \text{CH}_3, \text{C}_4\text{H}_9$) attached to the ionic heads, while compounds bearing larger chains ($R = \text{C}_{12}\text{H}_{25}, 4\text{-C}_6\text{H}_4\text{OC}_{12}\text{H}_{25}$) at the imidazolium head group favor the formation of smectic monolayers, possibly due to steric hindrance. A similar behavior has been observed for 5-phenylpyrimidine derivatives.²⁴ The tightest packing of the molecules within the smectic bilayers was observed for compound *p*-6(12,8) ($d_{001}/L_{\text{calc.}} = 1.19$) with the *N*-butylimidazolium head group. A similar observation was made for the corresponding 5-phenylpyrimidine isomer.¹⁰

Although the use of *meta*-substituted 2-phenylpyrimidines *m*-5(12,*m*)–*m*-8(12,*m*) rather than *para*-substituted ones *p*-5(*n*,*m*)–*p*-8(*n*,*m*) indeed shifted the mesophases to lower

Table 2 Phase transition temperatures (°C) and transition enthalpies (kJ mol⁻¹) of compounds *m*-5(12,*m*)–*m*-8(12,*m*) with different side chains, tether lengths and *N*-substituents^a

Entry	Compd	R ¹	Cr	SmA	I	Heating
1	<i>m</i> -5(12,4)	CH ₃	• 81 (3.4)	• 185 (0.6)	•	2. Heating
2	<i>m</i> -5(12,8)	CH ₃	• 52 (8.4)	• 134 (0.4)	•	2. Heating
3	<i>m</i> -6(12,4)	C ₄ H ₉	• 38 (7.1)	—	•	2. Heating
4	<i>m</i> -6(12,8)	C ₄ H ₉	• 40 (33.3)	• 89 (2.2)	•	2. Heating
5	<i>m</i> -7(12,4)	C ₁₂ H ₂₅	• 55 (0.9)	• 88 (1.5)	•	2. Heating
6	<i>m</i> -7(12,8)	C ₁₂ H ₂₅	• 50 (1.7)	• 54 (3.3)	•	2. Heating
7	<i>m</i> -8(12,4)	Ar	• 125 (11.7)	• 157 (1.2)	•	2. Heating
8	<i>m</i> -8(12,8)	Ar	• 91 (21.0)	• 108 (1.5)	•	2. Heating

^a Ar = C₁₂H₂₅OC₆H₄, Cr = crystalline, SmA = smectic A, and I = isotropic. Dot = phase was observed; dash = phase was not observed.

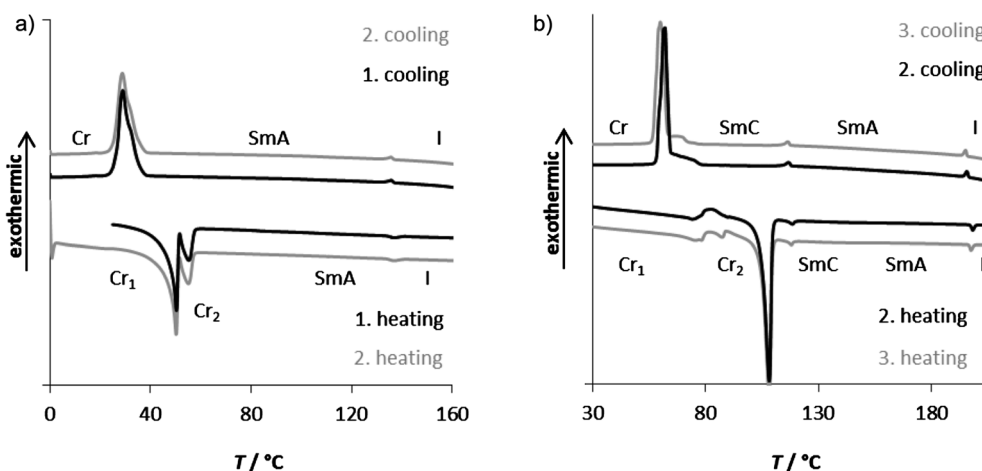


Fig. 1 DSC traces of (a) bent compound *m*-5(12,8) and (b) compound *p*-5(12,8), displaying a smectic C phase (heating/cooling rate: 10 K min⁻¹).

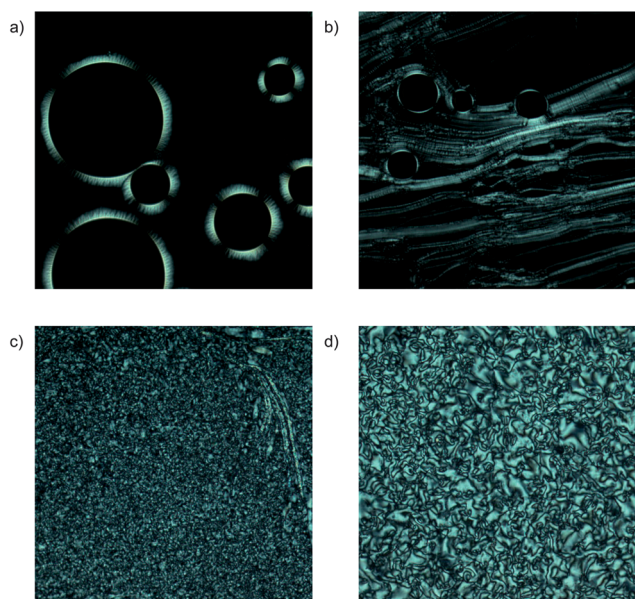


Fig. 2 Compounds *p*-5(10,8) and *p*-5(12,8) under crossed polarizers upon cooling from the isotropic melt (magnification $\times 200$): (a) homeotropic alignment and dichroism of *p*-5(10,8) at the air-liquid interface at 160 °C (cooling rate 10 K min⁻¹); (b) lamellar texture generated by shearing of *p*-5(10,8) at 160 °C (cooling rate 10 K min⁻¹); (c) unspecific texture of compound *p*-5(12,8) observed at the phase transition from SmA to SmC at 110 °C (cooling rate 5 K min⁻¹); (d) Schlieren texture of *p*-5(12,8) typical for a SmC phase (at 105 °C, cooling rate 5 K min⁻¹).

temperatures, we anticipated that this beneficial effect of tilting the mesogenic unit might be further extended, if the phenyl moiety is replaced by a bent and more flexible carboxylic ester moiety.

Thus, the sodium salt of 3,3-dimethoxy-2-methoxy-carbonylpropen-1-ol **18**²⁵ was treated with tetradecanamide **10b** to give the desired methyl-2-tetradecylpyrimidine-5-carboxylate **19**, which was submitted to saponification,²⁶ followed by esterification with ω -bromo- α -alcohols under Steglich conditions²⁷ to give bromoalkyl pyrimidine-5-carboxylates **20(m)**. Subsequent treatment with *N*-alkylimidazole **13a,c,d** yielded the target products **21(m)**–**26(m)** (Scheme 5).

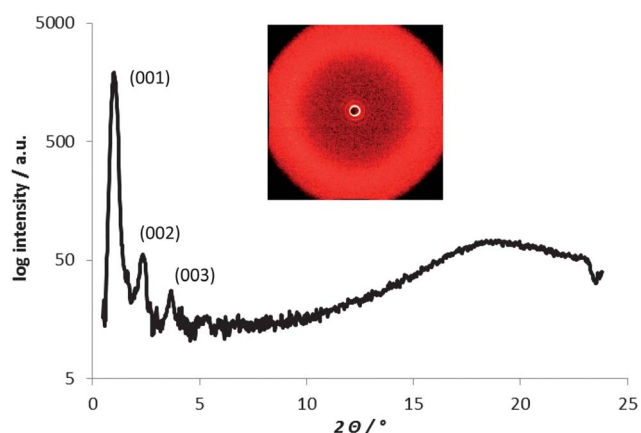


Fig. 3 SAXS plot and WAXS diffractogram (inset) of compound *p*-5(12,8) within the SmC phase (both at 110 °C).

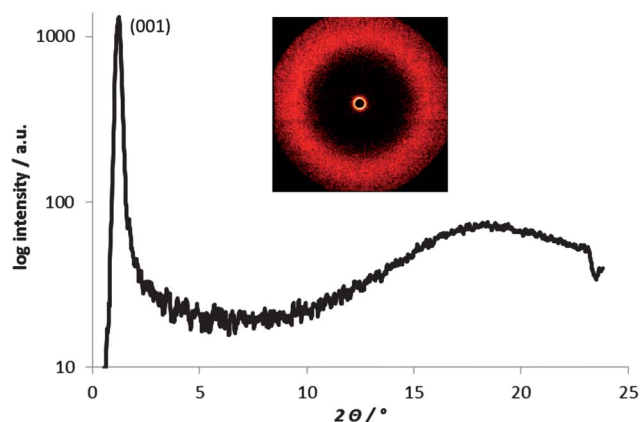


Fig. 4 SAXS plot and WAXS diffractogram (inset) of compound *p*-5(12,8) within the SmA phase (both at 190 °C).

Again, mesomorphic properties were studied by DSC (Table 4).

Indeed, 2-pyrimidine carboxylates **21(m)** and **22(m)** showed melting points in the range of 41 to 55 °C independent of the spacer length or the *N*-substituent and decreased clearing points with increasing spacer lengths and/or *N*-substituent (entries 1–4).

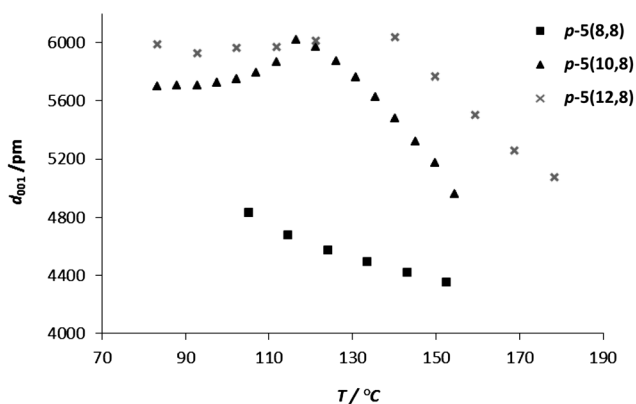


Fig. 5 Temperature dependence of the layer spacing for compounds *p*-5(8,8)–*p*-5(12,8).

In the case of *N*-4-dodecyloxyphenylimidazolium derivatives **23**(4) and **23**(8) the transition temperatures are still relatively high (entries 5 and 6). However, the high clearing temperatures of **21**(4), **21**(8) and **23**(4) resulted in decomposition after prolonged heating or repetitive heating/cooling cycles.

In order to avoid this thermal decomposition we decided to replace bromide by triflate, because literature precedence attributed this counter ion a beneficial effect on the thermal stability.²⁸ We were pleased to find that the *N*-methyl and *N*-dodecylimidazolium triflates **23**(4), **24**(8) and **25**(4) indeed showed the SmA phase at or slightly above room temperature and clearing temperatures between 73 and 142 °C (entries 7–9). Table 4 also shows the balanced influence between the spacer and the *N*-substituent. While short C4 spacer/*N*-methyl resulted in clearing transition at 142 °C, the combination C8 spacer/*N*-methyl decreased the clearing transition to 79 °C. The combination C4 spacer/*N*-dodecyl decreased the clearing temperature to 73 °C. Again the long/long combination, *i.e.* C8 spacer/*N*-dodecyl turned out to be unfavourable for mesophase formation

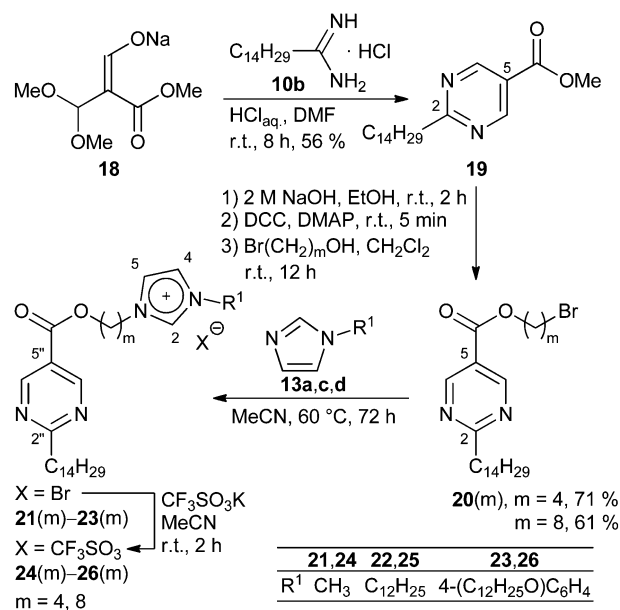
Table 3 XRD data of representative 2-phenylpyrimidines *p*-5(*n,m*)–*p*-8(*n,m*) and *m*-5(12,*m*)–*m*-8(12,*m*) assigned type of mesophase and proposed packing within the mesophases

Compound	R ¹	Phase type ^a	<i>L</i> _{calc} ^b /pm	<i>d</i> ₀₀₁ ^c /pm	<i>d</i> ₀₀₁ ^c / <i>L</i> _{calc}	<i>L</i> _{XRD} ^f /pm
<i>p</i> -5(12,4)	CH ₃	SmA ₂	3200	4501 ^c	1.41	2250
<i>p</i> -5(8,8)	CH ₃	SmA ₂	3200	4416 ^c	1.38	2208
<i>p</i> -5(10,8)	CH ₃	SmA ₂	3400	4633 ^c	1.35	2317
		SmA ₂	3400	6432 ^d	1.89	3216
		SmC ₂		5724 ^e	1.68	2862
<i>p</i> -5(12,8)	CH ₃	SmA ₂	3700	5115 ^c	1.39	2558
		SmA ₂	3700	6486 ^d	1.75	2558
		SmC ₂		5982 ^e	1.62	2991
<i>p</i> -6(12,8)	C ₄ H ₉	SmA ₂	4000	4746 ^c	1.19	2373
<i>p</i> -7(12,4)	C ₁₂ H ₂₅	SmA	4500	3540 ^c	0.79	3540
<i>p</i> -8(12,4)	Ar	SmA	5000	3675 ^c	0.74	3675
<i>m</i> -5(12,4)	Me	SmA ₂	3200	4053 ^c	1.27	2027
<i>m</i> -7(12,4)	C ₁₂ H ₂₅	SmA	2900	2767	0.95	2767

^a The subscript 2 in SmA₂ and SmC₂ indicates the formation of bilayers.

^b Molecular length calculated for *all-trans* configuration (calculated with Chem3D).²³ ^c *d*₀₀₁ at *T* = 0.95 × *T*_{iso} (after linear interpolation of data).

^d *d*₀₀₁ at *T* = 1.05 × *T*_{SmC/SmA} (after linear interpolation of data). ^e *d*₀₀₁ at *T* = 0.95 × *T*_{SmC/SmA} (after linear interpolation of data). ^f Layer spacing *L*_{XRD} = *d*₀₀₁ for monolayers, *L*_{XRD} = 0.5 × *d*₀₀₁ for bilayers.



Scheme 5

(entry 10). Both *N*-(dodecyloxyphenyl)imidazolium triflates **26**(4) and **26**(8) also displayed SmA mesophases albeit with higher melting points than those of **24**(*m*) and **25**(*m*), but comparable clearing points (entries 11 and 12).

Under POM typical Bättonnet textures together with homeotropic textures were observed upon cooling. As an example textures of compound **26**(4) are shown in Fig. 6.

The temperature-dependency of the layer spacing was investigated for **30b**, **31a** and **32a** upon cooling from the isotropic melt (Fig. 7).

Upon increasing temperature the layer spacings of **24**(8), **25**(4) and **26**(4) became smaller due to the simultaneous decrease of orientational order. This behaviour is typical for SmA phases and confirms the above-proposed assignment of the mesophase type of the triflate compounds.²⁹ As described above, the *d*₀₀₁ values at a reduced temperature were determined in order to compare them with the calculated length of the molecules (Table 5).

The quotient of experimentally determined layer spacing and the calculated molecular length is smaller than 1 for compounds **25**(4) and **26**(4). SmA monolayers with strongly interdigitated alkyl chains are therefore proposed for both compounds (Fig. 8).

In contrast the corresponding value of 1.28 for compound **24**(8) reveals the formation of a bilayer structure within the mesophase (Fig. 9).

In agreement with the above-discussed 2-phenylpyrimidines the type of packing pattern depends on the *N*-substituent. For *N*-methyl a smectic bilayer is proposed and for *N*-4-dodecyloxyphenyl and *N*-dodecyl, smectic monolayers are proposed in agreement with the experimental data.

Experimental

General information

Solvents were dried and distilled under nitrogen prior to use and generally all reactions were carried out under a nitrogen atmosphere with Schlenk-type glassware. Flash chromatography was

Table 4 Phase transition temperatures (°C) and transition enthalpies (kJ mol⁻¹) of carboxylates **21(m)**–**26(m)**

Entry	Compound	R ¹	X	Cr	SmA	I	Heating		
1	21(4)	CH ₃	Br	•	44 (35.3)	•	237 (0.5)	•	1 ^{sta}
2	21(8)	CH ₃	Br	•	42 (53.0)	•	219 (1.0)	•	2 ^{nda}
3	22(4)	C ₁₂ H ₂₅	Br	•	41 (18.4)	•	164 (1.8)	•	2 nd
4	22(8)	C ₁₂ H ₂₅	Br	•	55 (35.2)	•	76 (1.3)	•	2 nd
5	23(4)	C ₁₂ H ₂₅ OC ₆ H ₄	Br	•	77 (78.5)	•	229 (2.6)	•	1 ^{sta}
6	23(8)	C ₁₂ H ₂₅ OC ₆ H ₄	Br	•	101 (18.2)	•	172 (2.6)	•	2 nd
7	24(4)^b	CH ₃	CF ₃ SO ₃	•	35 (19.2)	•	142 (0.6)	•	2 nd
8	24(8)^b	CH ₃	CF ₃ SO ₃	•	32 (19.9)	•	79 (0.3)	•	2 nd
9	25(4)^c	C ₁₂ H ₂₅	CF ₃ SO ₃	•	25 (21.0)	•	73 (1.1)	•	2 nd
10	25(8)	C ₁₂ H ₂₅	CF ₃ SO ₃	•	22	—	—	•	—
11	26(4)^c	C ₁₂ H ₂₅ OC ₆ H ₄	CF ₃ SO ₃	•	90 (19.0)	•	142 (2.1)	•	2 nd
12	26(8)^c	C ₁₂ H ₂₅ OC ₆ H ₄	CF ₃ SO ₃	•	49 (8.5)	•	72 (1.6)	•	2 nd

^a Decomposition after 1. heating. ^b Packing as smectic bilayers. ^c Packing as smectic monolayers. Cr = crystalline, SmA = smectic A, and I = isotropic. Dot = phase was observed; dash = phase was not observed.

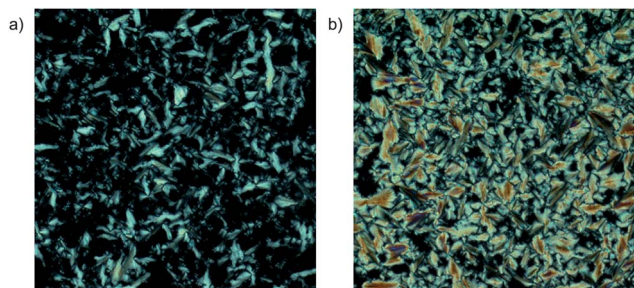


Fig. 6 Bâtonnet textures of compound **26(4)** under crossed polarizers upon cooling from the isotropic melt (magnification 200): (a) at 45 °C and (b) at 35 °C (cooling rate 10 K min⁻¹).

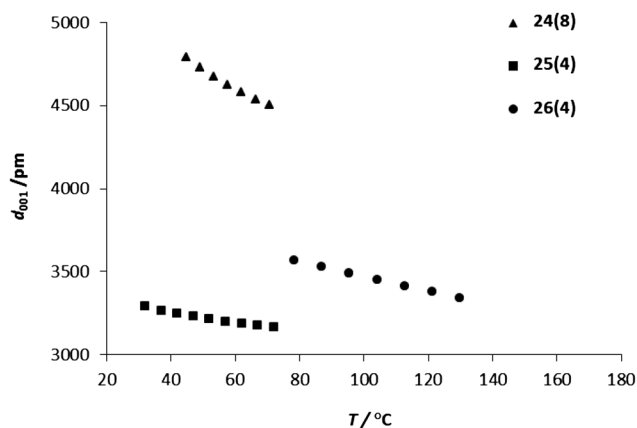


Fig. 7 Temperature dependent layer spacings of compounds **24(8)**, **25(4)** and **26(4)**.

Table 5 X-ray data for 2-pyrimidine carboxylates **24(8)**, **25(4)** and **26(4)**

Comp.	m	R ¹	X	Phase type ^a	L _{calc.} ^b /pm	d ₀₀₁ ^c /pm	d ₀₀₁ /L _{calc.}	L _{XRD} ^d /pm
24(8)	8	Me	CF ₃ SO ₃	SmA ₂	3400	4388	1.29	2194
25(4)	4	C ₁₂ H ₂₅	CF ₃ SO ₃	SmA	4200	3167	0.75	3167
26(4)	4	Ar	CF ₃ SO ₃	SmA	4700	3316	0.71	3316

^a The subscript 2 in SmA₂ indicates the formation of bilayers. ^b Molecular length calculated for all-trans configuration (calculated with Chem3D).²¹ ^c d₀₀₁ at T = 0.95 × T_{iso} (after linear interpolation of data). ^d Layer spacing L_{XRD} = d₀₀₁ for monolayers, L_{XRD} = 0.5 × d₀₀₁ for bilayers.

performed on silica gel, grain size 40–63 μm (*Fluka*). Thin layer chromatography (TLC) was done on aluminium sheets pre-coated with silica gel 60 F₂₅₄ (*Merck*). The obtained chromatograms were visualized by UV-light (λ = 254 nm) to determine the retention factors (R_f).

The following instruments were used for characterization of the compounds. NMR: *Bruker Avance 250* (¹H, 250 MHz; ¹³C, 63 MHz) and *Bruker Avance 500* (¹H, 500 MHz; ¹³C, 126 MHz). ¹H and ¹³C NMR spectra were referenced to TMS (Me₄Si δ_H = 0.0 ppm, δ_C = 0.0 ppm) as an internal standard. Unless otherwise stated, spectra were recorded at room temperature. Chemical shift calculations and 2D experiments (COSY and HMBC) supported the assignments of the resonances. Elemental analyses: Carlo Erba Strumentazione Elemental Analyzer, Modell 1106. IR: *Bruker Vector 22* FT-IR Spectrometer with MKII golden gate single reflection Diamant ATR system. MS (EI): *Varian MAT 711* spectrometer. MS (ESI): *Bruker Daltonics microTOF-Q* spectrometer. Differential scanning calorimetry (DSC): *Mettler-Toledo DSC 822e* (heating/cooling rates were 5 K min⁻¹). Polarizing optical microscopy: *Olympus BX50* polarizing microscope combined with a *Linkam TP93* central controller. X-ray diffraction (WAXS, SAXS regions): *Bruker AXS Nanostar C* diffractometer employing Ni-filtered CuK_α radiation (λ = 1.5418 Å). Melting points: *Büchi SMP-20*.

Full characterization of selected new compounds *p-5(12,8)*, *m-5(12,8)*, **21(8)** and **24(8)** is given below. For all other compounds see the ESI.†

General procedure for the preparation of alkyimidazolium bromides **4**, *p-5(n,m)*–*p-6(n,m)*, *m-5(n,m)*–*m-6(n,m)* and **21(m)**

To a solution of the respective bromide **12**, *p-17(n,m)*, *m-17(12,m)* or **20(m)** (1.00 mmol) in abs. acetonitrile was added

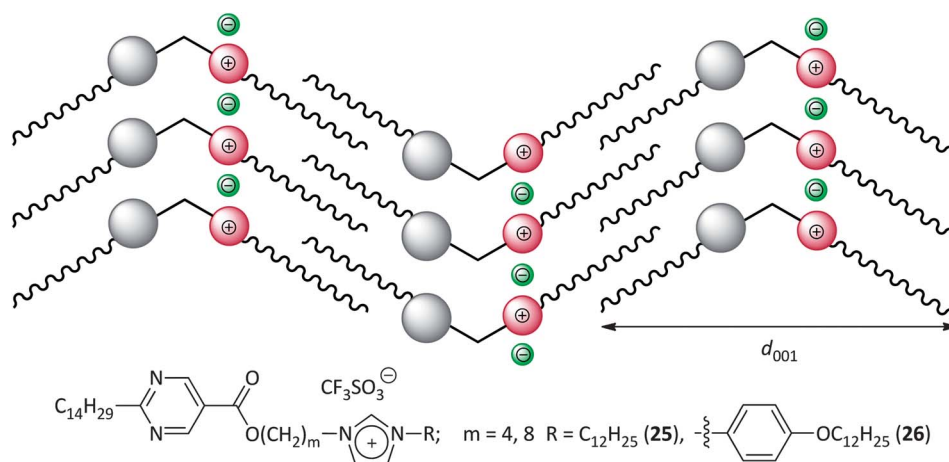


Fig. 8 Schematic illustration of a smectic monolayer *e.g.* formed by compounds **25**(4) and **26**(4).

freshly distilled *N*-methylimidazole **13a** or *N*-butylimidazole **13b** (10.0 mmol) and the reaction mixture was stirred at 60 °C for a given time. Then the mixture was added dropwise in EtOAc (10 mL), the precipitate was filtered off and washed with EtOAc (3 × 10 mL). The precipitate was dried over P_4O_{10} to give the imidazolium salts as colourless solids.

3-Methyl-1-{4-[4-(5-dodecylpyrimidin-2-yl)phenoxy]octyl}imidazolium bromide (*p*-5(**12,8**))

From *p*-**17**(12,8) (0.19 mmol, 100 mg) and **13a** (1.88 mmol, 154 mg) in abs. DMF (2 mL), reaction time: 120 h; yield: 84.0 mg (73%), colourless solid. Found: C, 66.60; H, 8.49; N, 9.11%. $C_{34}H_{53}BrN_4O$ requires C, 66.54; H, 8.70; N, 9.13%; M, 585.66. FT-IR (ATR): ν_{max}/cm^{-1} 3141 (w), 3032 (w), 2920 (s), 2849 (m), 2193 (w), 1608 (m), 1582 (m), 1540 (w), 1514 (w), 1469 (w), 1430 (s), 1395 (w), 1330 (w), 1303 (w), 1251 (s), 1179 (m), 1167 (m),

1108 (w), 1064 (w), 1036 (m), 996 (w), 946 (w), 909 (w), 845 (m), 818 (w), 799 (m), 786 (w), 772 (w), 756 (w), 729 (m), 652 (w), 623 (w), 611 (w). δ_H (250 MHz, $CDCl_3$) 0.81 (t, 3H, $J = 6.6$ Hz, CH_3), 1.11–1.46 (m, 26H, CH_2), 1.50–1.64 (m, 2H, NCH_2CH_2), 1.66–1.78 (m, 2H, $5'''-CH_2CH_2$), 1.79–1.94 (m, 2H, OCH_2CH_2), 2.45–2.60 (m, 2H, $5'''-CH_2$), 3.95 (t, 2H, $J = 6.4$ Hz, OCH_2), 4.05 (s, 3H, NCH_3), 4.25 (t, 2H, $J = 7.5$ Hz, CH_2N), 6.85–6.97 (m, 2H, $3''-H$, $5''-H$), 7.15–7.32 (m, 2H, 4-H, 5-H), 8.22–8.33 (m, 2H, $2''-H$, $6''-H$), 8.50 (s, 2H, $4'''-H$, $6'''-H$), 10.59 (s, 1H, 2-H) ppm. δ_C (125 MHz, $CDCl_3$) 14.1 (CH_3), 22.7, 25.9, 26.1, 28.8, 29.0, 29.1, 29.3, 29.5, 29.6, 30.2, 30.8, 31.9 (CH_2) 36.8 (NCH_3), 50.2 (CH_2N), 67.9 (OCH_2), 114.4 ($C-3''$, $C-5''$), 121.5 ($C-4$), 123.1 ($C-5$), 129.4 ($C-2''$, $C-6''$), 130.2 ($C-1''$), 132.2 ($C-2$), 138.2 ($C-5'''$), 157.0 ($C-4'''$, $C-6'''$), 161.1 ($C-4''$), 162.4 ($C-2'''$) ppm. MS (ESI): $m/z = 533.4$ [$M - Br$] $^+$. HRMS (ESI): m/z calcd for $C_{34}H_{53}N_4O^+$: 533.4214, found: 533.4210 [$M - Br$] $^+$. DSC: Cr 104 °C [48.0 kJ mol $^{-1}$] SmC 116 °C [0.6 kJ mol $^{-1}$] SmA 197 °C

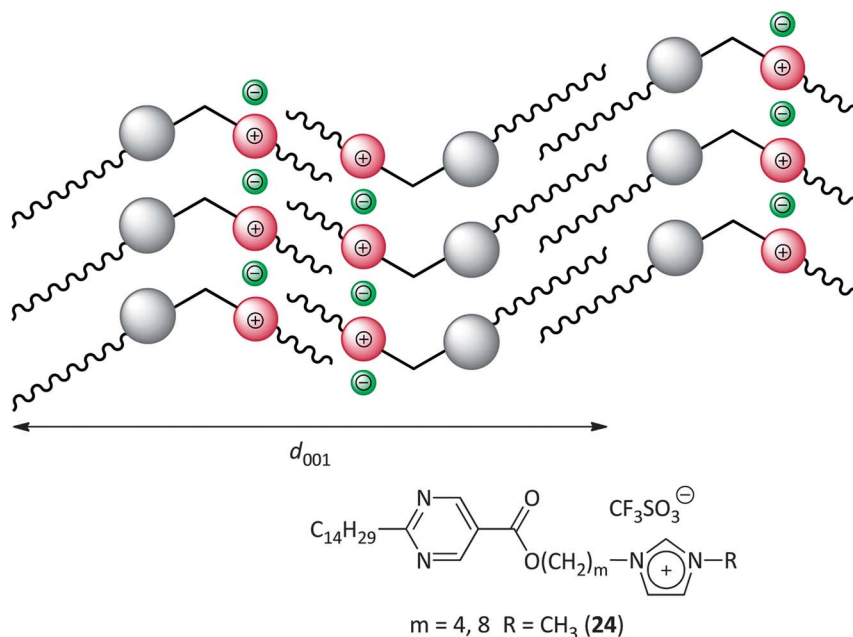


Fig. 9 Schematic illustration of a smectic bilayer, *e.g.* formed by compound **24**(8).

[0.7 kJ mol⁻¹] I (2nd heating); I 197 °C [-0.7 kJ mol⁻¹] SmA 118 °C [-0.6 kJ mol⁻¹] SmC 64 °C [-47.1 kJ mol⁻¹] Cr (2nd cooling).

1-{4-[3-(5-Dodecylpyrimidin-2-yl)phenoxy]octyl}-3-methylimidazolium bromide (*m*-5(12,8))

From *m*-17(12,8) (0.081 mmol, 43.0 mg) and **13a** (0.81 mmol, 67.0 mg), 72 h; yield: 35.0 mg (71%). Found: C, 64.83; H, 8.83; N, 8.54%. C₃₄H₅₃BrN₄O₂ requires C, 66.54; H, 8.70; N, 9.13%; M, 613.71. FT-IR (ATR): $\nu_{\max}/\text{cm}^{-1}$ 3081 (w), 2953 (w), 2919 (s), 2849 (m), 1608 (w), 1581 (m), 1542 (m), 1469 (m), 1447 (m), 1426 (s), 1395 (w), 1328 (m), 1296 (m), 1252 (w), 1234 (w), 1205 (m), 1169 (m), 1087 (w), 1045 (m), 948 (w), 902 (w), 882 (w), 825 (w), 811 (w), 778 (m), 755 (w), 722 (m), 692 (m), 651 (w), 619 (w), 561 (w), 544 (w), 520 (w). δ_{H} (500 MHz, CDCl₃) 0.81 (t, 3H, *J* = 6.5 Hz, CH₃), 1.03–1.47 (m, 6H, CH₂), 1.80–1.94 (m, 2H, CH₂), 2.49–2.63 (m, 2H, 5'''-CH₂), 3.99 (t, 2H, *J* = 6.4 Hz, OCH₂), 4.05 (s, 3H, NCH₃), 4.25 (t, 2H, *J* = 7.4 Hz, NCH₂), 6.89–7.00 (m, 1H, 6''-H), 7.13–7.24 (m, 2H, 4-H, 5-H), 7.31 (t, 1H, *J* = 7.9 Hz, 5''-H), 7.83–7.99 (m, 2H, 2''-H, 4''-H), 8.55 (s, 2H, 4'''-H, 6'''-H), 10.62 (s, 1H, 2-H) ppm. δ_{C} (125 MHz, CDCl₃) 14.1 (CH₃), 22.7, 25.9, 26.1, 28.8, 29.0, 29.1, 29.2, 29.3, 29.5, 29.6, 30.2, 30.8, 31.9 (CH₂), 36.8 (NCH₃), 50.2 (CH₂N), 67.9 (OCH₂), 113.1 (C-2''), 117.3 (C-6''), 120.3, 121.4, 123.0 (C-4'', C-4, C-5), 129.6 (C-5''), 133.2 (C-3''), 138.3, 139.1 (C-2, C-5'''), 157.0 (C-4''', C-6'''), 159.5 (C-1''), 162.2 (C-2''') ppm. MS (ESI): *m/z* = 533.4 [M – Br]⁺. HRMS (ESI): *m/z* calcd for C₃₀H₅₃N₄O⁺: 533.4214, found: 533.4204 [M – Br]⁺. DSC: Cr 81 °C [3.4 kJ mol⁻¹] SmA 185 °C [0.6 kJ mol⁻¹] I (2nd heating), I 184 °C [-0.7 kJ mol⁻¹] SmA (2nd cooling); no recrystallization was observed upon cooling.

3-Methyl-1-(8-((2-tetradecylpyrimidin-5-yl)carbonyl)oxy)octyl)imidazolium bromide (**21(8)**)

From **20(8)** (0.16 mmol, 80.0 mg) and **13a** (1.60 mmol, 131 mg), 72 h; yield: 50.0 mg (49%). Found: C, 61.42; H, 8.88; N, 9.04%. C₃₁H₅₃BrN₄O₂ requires C, 62.72; H, 9.00; N, 9.44%; M, 593.34. FT-IR (ATR): $\nu_{\max}/\text{cm}^{-1}$ 3068 (w), 2923 (s), 2853 (m), 1723 (s), 1590 (s), 1551 (m), 1466 (m), 1442 (m), 1390 (m), 1290 (s), 1169 (m), 1134 (m), 1037 (w), 909 (s). δ_{H} (500 MHz, CDCl₃) 0.88 (t, 3H, *J* = 7.1 Hz, CH₃), 1.21–1.46 (m, 24H, CH₂), 1.73–1.87 (m, 4H, CH₂), 1.90–1.99 (m, 2H, CH₂), 2.99–3.05 (m, 2H, 2-CH₂), 4.14 (s, 3H, CH₃), 4.35 (t, 2H, *J* = 6.9 Hz, CH₂N), 7.29–7.39 (m, 2H, 4-H, 5-H), 9.18 (s, 2H, 4'-H, 6'-H), 10.67 (s, 1H, 2-H) ppm. δ_{C} (125 MHz, CDCl₃) 14.1 (CH₃), 22.7, 25.8, 26.2, 28.5, 28.9, 29.36, 29.38, 29.41, 29.5, 29.6, 29.65, 29.68, 29.69, 30.3, 31.9, 36.8 (CH₂), 39.8 (2'-CH₂), 50.2 (CH₂N), 65.6 (OCH₂), 121.4, 121.5 (C-4, C-5), 123.1 (C-5'), 138.3 (C-1), 158.1 (C-4', C-6'), 164.1 (CO₂), 175.3 (C-2') ppm. MS (ESI): *m/z* = 513.4 [M – Br]⁺, 321.3, 193.2, 83.1. HRMS (ESI): *m/z* calcd for C₃₁H₅₃N₄O₂⁺: 513.4163, found: 513.4153 [M – Br]⁺. DSC: Cr 42 °C [53.0 kJ mol⁻¹] SmA 219 °C [1.0 kJ mol⁻¹] I (1st heating); decomposition upon clearing.

1-(8-((2-Tetradecylpyrimidin-5-yl)carbonyl)oxy)octyl)-3-[4-(dodecyloxy)phenyl]imidazolium bromide (**23(8)**)

From **20(8)** (0.14 mmol, 70.0 mg) and **13d** (0.27 mmol, 90.0 mg), 72 h; yield: 105 mg (91%). Found: C, 68.61; H, 9.25; N, 6.61%. C₄₈H₇₉BrN₄O₃ requires C, 68.63; H, 9.48; N, 6.67%; M, 840.07.

FT-IR (ATR): $\nu_{\max}/\text{cm}^{-1}$ 3046 (w), 2920 (s), 2851 (m), 1720 (s), 1590 (s), 1551 (m), 1516 (w), 1469 (m), 1442 (m), 1394 (w), 1289 (s), 1257 (m), 1136 (m), 1075 (w). δ_{H} (500 MHz, CDCl₃) 0.88 (t, 6H, *J* = 6.9 Hz, 2 × CH₃), 1.19–1.50 (m, 48H, CH₂), 1.73–1.87 (m, 6H, CH₂), 1.96–2.05 (m, 2H, CH₂), 2.98–3.06 (m, 2H, 2-CH₂), 3.98 (t, 2H, *J* = 6.6 Hz, OCH₂), 4.35 (t, 2H, *J* = 6.9 Hz, NCH₂), 4.60 (t, 2H, *J* = 7.3 Hz, CH₂N), 7.01–7.06 (m, 2H, 3'''-H, 5'''-H), 7.39–7.52 (m, 2H, 4-H, 5-H), 7.66–7.70 (m, 2H, 2'''-H, 6'''-H), 9.17 (s, 2H, 4''-H, 6''-H), 11.15 (s, 1H, 2-H) ppm. δ_{C} (125 MHz, CDCl₃) 14.1 (CH₃), 22.7, 25.8, 26.0, 26.2, 28.5, 28.6, 28.91, 28.94, 29.1, 29.36, 29.42, 29.5, 29.57, 29.60, 29.62, 29.66, 29.68, 30.4, 31.90 (CH₂), 39.8 (2''-CH₂), 50.4 (CH₂N), 65.6, 68.7 (2 × OCH₂), 116.1 (C-3''', C-5'''), 120.3 (C-5''), 121.5, 122.0 (C-4, C-5), 123.3 (C-2''', C-6'''), 127.1 (C-1'''), 136.5 (C-2), 158.1 (C-4'', C-6''), 160.5 (C-4'''), 164.1 (CO₂), 175.3 (C-2'') ppm. MS (ESI): *m/z* = 759.6 [M – Br]⁺, 591.4, 439.4, 329.3. HRMS (ESI): *m/z* calcd for C₄₈H₇₉N₄O₃⁺: 759.6147, found: 759.6152 [M – Br]⁺. DSC: Cr₁ 31 °C [7.9 kJ mol⁻¹] Cr₂ 101 °C [18.2 kJ mol⁻¹] SmA 172 °C [2.6 kJ mol⁻¹] I (2nd heating); I 172 °C [-2.3 kJ mol⁻¹] SmA 76 °C [-14.4 kJ mol⁻¹] 36 °C [-8.3 kJ mol⁻¹] (2nd cooling).

General procedure for the preparation of trifluoromethanesulfonates **24(m)**–**26(m)**

To a solution of the respective compounds **21(m)**–**23(m)** (1.00 mmol) in acetonitrile (5 mL) at room temperature was added potassium trifluoromethanesulfonate (1.10 mmol), whereby colourless KBr precipitated. The reaction mixture was stirred for 2 h (tlc control). After completion of the reaction, the solvent was removed under vacuum. The residue was taken up in CH₂Cl₂ (5 mL) and filtered. The products were obtained as colourless solids without further purification.

3-Methyl-1-(8-((2-tetradecylpyrimidin-5-yl)carbonyl)oxy)octyl)imidazolium trifluoromethanesulfonate (**24(8)**)

From **21(8)** (0.068 mmol, 40.0 mg); yield: 45.0 mg (quant.). FT-IR (ATR): $\nu_{\max}/\text{cm}^{-1}$ 2924 (s), 2853 (m), 1724 (s), 1590 (s), 1442 (m), 1391 (m), 1259 (s), 1161 (m), 1031 (w), 904 (s)¹. δ_{H} (500 MHz, CDCl₃) 0.88 (t, 3H, *J* = 6.9 Hz, CH₃), 1.19–1.47 (m, 28H, CH₂), 1.73–1.95 (m, 6H, CH₂), 2.98–3.07 (m, 2H, 2-CH₂), 4.00 (s, 3H, CH₃), 4.21 (t, 2H, *J* = 7.6 Hz, OCH₂), 4.35 (t, 2H, *J* = 6.6 Hz, OCH₂), 7.24–7.32 (m, 2H, 4-H, 5-H), 9.17 (s, 2H, 4'-H, 6'-H), 9.28 (s, 1H, 2-H) ppm. δ_{C} (125 MHz, CDCl₃) 14.1 (CH₃), 22.7, 25.7, 26.1, 28.5, 28.6, 28.8, 28.9, 29.36, 29.38, 29.42, 29.5, 29.6, 29.65, 29.69, 30.0, 31.9, 36.6 (CH₂), 39.8 (2'-CH₂), 50.2 (CH₂N), 65.6 (OCH₂), 121.5, 121.8 (C-4, C-5), 121.9 (CF₃), 123.3 (C-5'), 137.4 (C-1), 158.1 (C-4', C-6'), 164.1 (CO₂), 175.3 (C-2') ppm. MS (ESI, positive): *m/z* = 513.4 [M – CF₃SO₃]⁺, 321.3, 193.2, 83.1. MS (ESI, negative): *m/z* = 149.0 [CF₃SO₃]⁻, 99.0, 80.0. HRMS (ESI, positive): *m/z* calcd for C₃₁H₅₃N₄O₂⁺: 513.4163, found: 513.4177 [M – CF₃SO₃]⁺. HRMS (ESI, negative): *m/z* calcd for CF₃SO₃⁻: 148.9515, found: 148.9527 [CF₃SO₃]⁻. DSC: Cr₁ 9 °C [12.8 kJ mol⁻¹] Cr₂ 32 °C [19.9 kJ mol⁻¹] SmA 79 °C [0.3 kJ mol⁻¹] I (2nd heating), I 84 °C [-0.3 kJ mol⁻¹] SmA 35 °C [-20.3 kJ mol⁻¹] Cr₂ 1 °C [-6.6 kJ mol⁻¹] Cr₁ (2nd cooling).

1-(8-((2-Tetradecylpyrimidin-5-yl)carbonyloxy)octyl)-3-[4-(dodecyloxy)phenyl]imidazolium trifluoromethanesulfonate (26(8))

From **23(8)** (0.071 mmol, 60.0 mg); yield: 65.0 mg (quant.). FT-IR (ATR): $\nu_{\max}/\text{cm}^{-1}$ 2921 (s), 2852 (m), 1725 (s), 1591 (s), 1554 (m), 1514 (s), 1468 (m), 1391 (m), 1256 (s), 1160 (m), 1031 (w). δ_{H} (500 MHz, CDCl_3) 0.87 (t, 3H, $J = 7.0$ Hz, $2 \times \text{CH}_3$), 1.18–1.51 (m, 48H, CH_2), 1.73–1.87 (m, 6H, CH_2), 1.89–1.99 (m, 2H, CH_2), 2.98–3.06 (m, 2H, 2- CH_2), 3.99 (t, 2H, $J = 6.3$ Hz, CH_2N), 4.35 (t, 2H, $J = 6.6$ Hz, OCH_2), 4.39 (t, 2H, $J = 7.6$ Hz, CH_2N), 7.01–7.06 (m, 2H, 3'''-H, 5'''-H), 7.40–7.51 (m, 2H, 2'''-H, 6'''-H), 7.52–7.56 (m, 2H, 4-H, 5-H), 9.17 (s, 2H, 4''-H, 6''-H), 9.61 (s, 1H, 2-H) ppm. δ_{C} (125 MHz, CDCl_3) 14.1 (CH_3), 22.7, 25.7, 26.0, 26.1, 28.5, 28.6, 28.8, 28.9, 29.1, 29.36, 29.42, 29.52, 29.57, 29.60, 29.65, 29.7, 30.2, 31.9 (CH_2), 39.8 (2''- CH_2), 50.6 (CH_2N), 65.6, 68.7 (OCH_2), 116.1 (C-3''', C-5'''), 121.1 (C-5'''), 121.4 (CF_3), 121.3, 122.5 (C-4, C-5), 123.5 (C-2''', C-6'''), 127.0 (C-1'''), 135.4 (C-2), 158.1 (C-4'', C-6''), 160.7 (C-4'''), 164.1 (CO_2), 175.3 (C-2'') ppm. MS (ESI, positive): $m/z = 759.6$ [$\text{M} - \text{CF}_3\text{SO}_3$] $^+$, 591.4, 439.4, 329.3, 271.2, 161.1. MS (ESI, negative): $m/z = 149.0$ [CF_3SO_3] $^-$, 99.0, 80.0. HRMS (ESI, positive): m/z calcd for $\text{C}_{48}\text{H}_{79}\text{N}_4\text{O}_3^+$: 759.6147, found: 759.6131 [$\text{M} - \text{CF}_3\text{SO}_3$] $^+$. HRMS (ESI, negative): m/z calcd for $\text{CF}_3\text{O}_3\text{S}^-$: 148.9515, found: 148.9523 [CF_3SO_3] $^-$. DSC: Cr₁ 21 °C [−17.7 kJ mol^{−1}] Cr₂ 44 °C [36.1 kJ mol^{−1}] Cr₃ 49 °C [8.5 kJ mol^{−1}] SmA 72 °C [1.6 kJ mol^{−1}] I (2nd heating); I 72 °C [−1.7 kJ mol^{−1}] SmA 29 °C [−16.7 kJ mol^{−1}] Cr₂ 17 °C [−10.6 kJ mol^{−1}] Cr₁ (2nd cooling).

Conclusions

Two series of new compounds, imidazolium bromides with mesogenic 2-phenylpyrimidine *p*-5(*n,m*)-*p*-8(*n,m*) and 2-alkylpyrimidinecarboxylic acid cores **21(m)**–**23(m)**, were investigated. As a general trend the liquid crystalline 2-phenylpyrimidines *p*-5(*n,4*)-*p*-8(*n,4*) with a C4 spacer exhibited smectic A mesophases. Elongation of the spacer to C8 generally leads to a small decrease of melting and a significant decrease of clearing temperatures. Surprisingly two of the derivatives with the longer spacer (*p*-5(10,8), *p*-5(12,8)) also displayed smectic C phases. 2-Phenylpyrimidines *p*-5(*n,m*)-*p*-8(*n,m*) exhibited smectic mesophases over a broad temperature range (up to $\Delta T = 143$ K), but the melting and clearing points are quite high. We therefore changed the molecular geometry from linear (*para*-substituted 2-phenylpyrimidines *p*-5(*n,m*)-*p*-8(*n,m*)) to bent and synthesized a series of *meta*-substituted 2-phenylpyrimidines *m*-5(12,*m*)-*m*-8(12,*m*) with terminal C12 alkyl chains. The reduction of symmetry delivered the desired effect as all compounds *m*-5(12,*m*)-*m*-8(12,*m*) displayed lower melting and clearing temperatures compared to their linear isomers *p*-5(12,*m*)-*p*-8(12,*m*).

The second investigated series, the 2-alkylpyrimidinecarboxylic acid imidazolium bromides, exhibited smectic A mesophases, most of them over a very broad temperature range (up to $\Delta T = 193$ K). Unfortunately some of the compounds (**21(m)**, **23(4)**) decomposed at higher temperatures. To overcome this problem the bromide anion was exchanged with a triflate anion in a salt metathesis reaction. The resulting thermally stable derivatives **24(m)**–**26(m)** exhibited smaller mesophase ranges but melted near room temperature.

X-ray investigations of selected compounds of both series, 2-phenylpyrimidines and 2-alkylpyrimidinecarboxylic acids, suggest a general trend for the packing of the molecules within the smectic mesophases depending on the substitution pattern of the imidazolium head groups. Smectic bilayers comprised compounds with *N*-methyl or *N*-butyl groups attached to the imidazolium head groups while *N*-4-dodecyloxyphenyl and *N*-dodecyl derivatives displayed smectic monolayers.

In conclusion, the results revealed that for both 5- and 2-phenylpyrimidine ILCs bending of the mesogenic core unit, *i.e.* *meta* rather than *para* substitution at the phenyl ring indeed resulted in mesophases near to room temperature with sufficient thermal stability. Furthermore, the carboxylate seems to be a suitable surrogate for *meta*-substituted phenyl units in 2-phenylpyrimidines leading also to significantly decreased melting points particularly if triflate anions were used rather than bromides. Future work must demonstrate whether bending of the mesogenic core unit leads to a general approach towards room temperature ILCs.

Acknowledgements

Generous financial support by the Deutsche Forschungsgemeinschaft, the Fonds der Chemischen Industrie, the Bundesministerium für Bildung und Forschung (shared instrumentation grant), the Studienstiftung des Deutschen Volkes (fellowship for M.B.) and the Ministerium für Wissenschaft, Forschung und Kunst des Landes Baden-Württemberg is gratefully acknowledged.

References

- 1 Reviews on ILs: (a) *Electrodeposition from Ionic Liquids*, ed. F. Endres, A. P. Abbott and D. R. MacFarlane, Wiley-VCH, Weinheim, 2008; (b) *Ionic Liquids IIIA: Fundamentals, Progress, Challenges, and Opportunities*, ed. K. R. Seddon and R. D. Rogers, ACS Symp. Ser., American Chemical Society, Washington DC, 2005, vol. 901; (c) *Ionic Liquids IIIB: Fundamentals, Progress, Challenges, and Opportunities—Transformations and Processes*, ed. K. R. Seddon and R. D. Rogers, ACS Symp. Ser., American Chemical Society, Washington DC, 2005, vol. 902; (d) *Ionic Liquids in Synthesis*, ed. P. Wasserscheid and T. Welton, Wiley-VCH, Weinheim, 2nd edn, 2007; (e) J. Dupont, R. F. de Souza and P. A. Z. Suarez, *Chem. Rev.*, 2002, **102**, 3667–3692.
- 2 *Reviews on LCs: Handbook of Liquid Crystals*, ed. D. Demus, J. Goodby, G. W. Gray, H. W. Spiess and V. Vill, Wiley-VCH, Weinheim, 2008, vol. 1–3.
- 3 Reviews on ILCs: (a) K. V. Axenov and S. Laschat, *Materials*, 2011, **4**, 206–259; (b) T. Kato, N. Mizoshita and K. Kishimoto, *Angew. Chem.*, 2006, **118**, 44–74; *Angew. Chem., Int. Ed.*, 2006, **45**, 38–68; (c) K. Binnemans, *Chem. Rev.*, 2005, **105**, 4148–4204.
- 4 R. P. Lemieux, *Acc. Chem. Res.*, 2001, **34**, 845–853.
- 5 Review: (a) M. Hird, *Liq. Cryst.*, 2011, **38**, 1467–1493; recent examples: (b) A. Katsuragi, E. Inoue and T. Sasaki, *Mol. Cryst. Liq. Cryst.*, 2011, **548**, 107–119; (c) K. Takeuchi, Y. Takanishi, J. Yamamoto and A. Yoshizawa, *Liq. Cryst.*, 2010, **37**, 507–515; (d) P. K. Mandel, S. Haldar, A. Lapanik and W. Haase, *Jpn. J. Appl. Phys.*, 2009, **48**, 011501.
- 6 C. Adamo and V. Barone, *J. Chem. Phys.*, 1998, **108**, 664–675.
- 7 V. Barone, L. Comisso, F. Lelj and N. Russo, *Tetrahedron*, 1985, **41**, 1915–1918.
- 8 (a) J. C. Roberts, N. Kapernaum, Q. Song, D. Nonnenmacher, K. Ayub, F. Giesselmann and R. P. Lemieux, *J. Am. Chem. Soc.*, 2010, **132**, 364–370; (b) J. C. Roberts, N. Kapernaum, F. Giesselmann and R. P. Lemieux, *J. Am. Chem. Soc.*, 2008, **130**, 13842–13843; (c) J. C. Roberts, N. Kapernaum, F. Giesselmann, M. D. Wand and R. P. Lemieux, *J. Mater. Chem.*, 2008, **18**,

- 5301–5306; (d) M. P. Thompson and R. P. Lemieux, *J. Mater. Chem.*, 2007, **17**, 5068–5076; (e) L. Li, C. D. Jones, J. Magolan and R. P. Lemieux, *J. Mater. Chem.*, 2007, **17**, 2313–2318; (f) M. P. Thompson, T. Hegmann, M. D. Wand and R. P. Lemieux, *Liq. Cryst.*, 2007, **34**, 987–994; (g) C. S. Hartley, N. Kapernaum, J. C. Roberts, F. Giesselmann and R. P. Lemieux, *J. Mater. Chem.*, 2006, **16**, 2329–2337.
- 9 (a) C. Damm, G. Israel, T. Hegmann and C. Tschierske, *J. Mater. Chem.*, 2006, **16**, 1808–1816; (b) B. Neumann, T. Hegmann, C. Wagner, P. R. Ashton, R. Wolf and C. Tschierske, *J. Mater. Chem.*, 2003, **13**, 778–784.
- 10 G. Starkulla, M. Kaller, W. Frey, K. V. Axenov and S. Laschat, *Liq. Cryst.*, 2011, **38**, 1515–1529.
- 11 (a) N. V. Plechkova and K. R. Seddon, *Chem. Soc. Rev.*, 2008, **37**, 123–150; (b) T. Payagala, J. Huang, Z. S. Breitbach, P. S. Sharma and D. W. Armstrong, *Chem. Mater.*, 2007, **19**, 5848–5850; (c) K. N. Marsh, J. A. Boxall and R. Lichtenthaler, *Fluid Phase Equilib.*, 2004, **219**, 93–98.
- 12 D. Lloyd, C. Reichardt and M. Struthers, *Liebigs Ann. Chem.*, 1986, 1368–1379.
- 13 (a) C. E. Kwartler and P. Lucas, *J. Am. Chem. Soc.*, 1943, **65**, 354–355; (b) Commercially available from Aurora Fine Chemicals Ltd.
- 14 (a) G. F. Starkulla, E. Kapatsina, A. Baro, F. Giesselmann, S. Tussetschläger, M. Kaller and S. Laschat, *Beilstein J. Org. Chem.*, 2009, **5**, 63; (b) E. Kapatsina, M. Lordon, A. Baro and S. Laschat, *Synthesis*, 2008, 2551–2560.
- 15 V. Nair, D. E. Vietti and C. S. Cooper, *J. Am. Chem. Soc.*, 1981, **103**, 3030–3036.
- 16 (a) Commercially available from Alfa Aesar A Johnson Matthey Company; (b) A. D. Turner, S. V. Pizzo, G. Rozakis and N. A. Porter, *J. Am. Chem. Soc.*, 1988, **110**, 244–250.
- 17 Examples of ILC with SmC phases: (a) S. Kokmoto, Y. Hara and K. Kishikawa, *Tetrahedron Lett.*, 2010, **51**, 1508–1511; (b) K. Goossens, K. Lava, P. Nockemann, K. Van Hecke, L. Van Meervelt, P. Pattison, K. Binnemans and T. Cardinaels, *Langmuir*, 2009, **25**, 5881–5897; (c) R. G. Santos-Martell, A. Ceniceros-Olguín, L. Larios-López, R. J. Rodríguez-González, D. Navarro-Rodríguez, B. Donnio and D. Guillon, *Liq. Cryst.*, 2009, **36**, 787–797; (d) Q. Zhang, C. Shan, X. Wang, L. Chen, L. Niu and B. Chen, *Liq. Cryst.*, 2008, **35**, 1299–1305; (e) D. Tsiourvas, T. Felekis, Z. Sideratou and C. M. Paleos, *Liq. Cryst.*, 2004, **31**, 739–744; (f) S. Ujiie and K. Iimura, *Chem. Lett.*, 1994, 17–20; (g) L. Cui, V. Sapagovas and G. Lattermann, *Liq. Cryst.*, 2002, **29**, 1121–1132.
- 18 *Liquid Crystals: Experimental Study of Physical Properties and Phase Transitions*, ed. S. Kumar, Cambridge University Press, Cambridge, 2001.
- 19 J. P. F. Lagerwall and F. Giesselmann, *Phys. Rev. E: Stat., Nonlinear, Soft Matter Phys.*, 2002, **66**, 031703.
- 20 S. Urban, J. Przedmojski and J. Czub, *Liq. Cryst.*, 2005, **32**, 619–624.
- 21 P. H. J. Kouwer and T. M. Swager, *J. Am. Chem. Soc.*, 2007, **129**, 14042–14052.
- 22 S. Sauer, S. Saliba, S. Tussetschläger, A. Baro, W. Frey, F. Giesselmann, S. Laschat and W. Kantlehner, *Liq. Cryst.*, 2009, **36**, 275–299.
- 23 Molecular modelling was done with Chem3D Pro 2008 software.
- 24 G. Starkulla, Ph.D. thesis, University of Stuttgart, 2012, submitted.
- 25 P. Zhichkin, D. J. Fairfax and S. A. Eisenbeis, *Synthesis*, 2002, 720–722.
- 26 P. Schenone, L. Sansebastiano and L. Mosti, *J. Heterocycl. Chem.*, 1990, **27**, 295–305.
- 27 G. Höfle, W. Steglich and H. Vorbrüggen, *Angew. Chem.*, 1978, **90**, 602–615; *Angew. Chem., Int. Ed.*, 1978, **17**, 569–583.
- 28 M. Butschies, J. C. Haenle, S. Tussetschläger and S. Laschat, *Liq. Cryst.*, submitted.
- 29 (a) S. Urban, J. Przedmojski and J. Czub, *Liq. Cryst.*, 2005, **32**, 619–624; (b) J. P. F. Lagerwall, F. Giesselmann and M. D. Radcliffe, *Phys. Rev. E: Stat., Nonlinear, Soft Matter Phys.*, 2002, **66**, 031703.